

Far-infrared absorption spectra of water, ammonia, and chloroform calculated from instantaneous normal mode theory

J. T. Kindt and C. A. Schmuttenmaer

Department of Chemistry, Yale University, New Haven, Connecticut 06520-8107

(Received 24 October 1996; accepted 11 December 1996)

Instantaneous normal mode (INM) theory was used to calculate absolute far-infrared absorption spectra of water, ammonia, and chloroform. Three procedures for weighting the INM density of states to yield absorption intensities were tested against spectra based on dipole time correlation functions generated from molecular dynamics (MD) simulations. Weighting method I, which utilizes only the rotational character of a mode in determining its contribution to absorption, performed slightly better than method II, a more exact treatment which incorporates the extent to which a mode is IR-active. Method III, which includes the contributions of induced dipoles, was successful in describing the influence of induced dipoles on the far-infrared spectra of the model liquids. The contribution to absorption of unstable modes with imaginary frequencies was found to be significant at low frequencies, and was treated by a simple approximation. Agreement between INM theory and the MD analysis was quite good for chloroform and ammonia, but less so for water. Agreement with experimental data in the range of 4–100 cm^{-1} was generally poor, but no worse than that for the MD calculations, primarily reflecting the simple intermolecular potentials used rather than the computational method itself. © 1997 American Institute of Physics. [S0021-9606(97)50711-2]

I. INTRODUCTION

Understanding the intermolecular dynamics of the liquid phase and its influence on processes of chemical and biochemical interest has recently been an area of intense study.¹ This field has been stimulated in part by the development of new ultrafast spectroscopies sensitive to the low-frequency (1–600 cm^{-1}) region of the spectrum, such as optical heterodyne-detected Raman-induced Kerr effect spectroscopy (OHD-RIKES) (Refs. 2–4) and femtosecond terahertz (fs THz) pulse spectroscopy.^{5–8} Due to the absence of sharp, readily assignable features in low-frequency spectra of liquids, computer simulations have proven to be of critical importance in interpreting spectra measured in this region.^{9–13} Instantaneous normal mode (INM) methods^{14,15} in particular provide a powerful and physically appealing approach to this task. A great advantage of the INM formalism is that its description of intermolecular dynamics in terms of collective normal modes, which can be analyzed or visualized by a variety of methods, can provide physical insight that is not readily available from time correlation functions averaged over the course of a long simulation. Another advantage of the INM method is that because it gives an instantaneous picture it can be easily used to calculate spectra during non-equilibrium simulations. For instance, the INM method would be ideal for modeling a time-resolved experiment in which the far-infrared (FIR) absorption spectrum is probed by sub-picosecond FIR pulse spectroscopy following an ultrafast excitation of the liquid.

Methods for applying the INM formalism to OHD-RIKES (or low frequency Raman) spectra have previously been developed.^{15,16} In this study we describe INM methods for the calculation of FIR spectra and apply them to water, liquid ammonia, and chloroform. We find good agreement

between spectra calculated using INM methods and spectra calculated according to conventional formulas, except in the case of water, where the small moment of inertia about the in-plane, non-dipolar axis appears to adversely affect the INM picture. We show how the effects of electronic polarization can be incorporated into the INM technique, and compare the spectra generated by both methods with experimental results determined by sub-ps FIR pulse spectroscopy.

The calculation of intermolecular instantaneous normal modes has been described in detail.^{17,18} Briefly, by starting with a given instantaneous configuration of an equilibrated system of N molecules generated by classical molecular dynamics methods, we obtain normal modes by diagonalization of the $6N \times 6N$ Hessian matrix of second derivatives of the intermolecular potential energy with respect to the translational and rotational degrees of freedom. Each normal mode is represented by a $6N$ -dimensional eigenvector, with each element in the eigenvector representing the contribution of one molecular degree of freedom to the collective mode. Each mode has an associated eigenvalue, representing the square of the mode frequency. The INM spectrum is obtained by calculating the INM frequencies for multiple instantaneous configurations drawn from the course of a molecular dynamics (MD), Monte Carlo, or other simulation. Because the system is drawn from a thermodynamic ensemble and is not at its global potential energy minimum, some modes represent unstable barrier-crossing motions; that is, the region of the multidimensional potential energy surface occupied by the system has negative curvature with respect to some degrees of freedom. These unstable degrees of freedom appear as modes with imaginary frequencies. It has been common practice to either ignore these modes, or introduce instead an exponential damping term or other mecha-

nism to account for the structural relaxation associated with the unstable modes.¹⁵ Techniques for calculating diffusion coefficients have been derived which employ the unstable mode distribution, however.^{19,20} While disregarding the imaginary modes is appropriate for some applications, we have chosen to incorporate them into our treatment of the FIR spectra of polar liquids.

II. THEORETICAL BACKGROUND

A. INM calculations

We followed the procedure described by Cho *et al.*¹⁸ for calculation of instantaneous normal modes of non-linear molecules. Briefly, $6N$ mass-weighted coordinates $z_{n\mu}$ are defined for N molecules, with $\mu = \{1, 2, \dots, 6\}$ corresponding to space-fixed translations along x , y , and z , and rotations about the molecular x , y , and z axes for each molecule n . The Hessian matrix $D(\mathbf{R}_0)$ is calculated, with elements

$$D_{n\mu, n'\mu'}(\mathbf{R}_0) = \frac{\partial}{\partial z_{n\mu}} \left(\frac{\partial V}{\partial z_{n'\mu'}} \right), \quad (1)$$

where V is the intermolecular potential at the instantaneous configuration \mathbf{R}_0 . Standard methods²¹ for diagonalization of $D(\mathbf{R}_0)$ yield a set of $6N$ eigenvalues λ_i and a $6N \times 6N$ unitary diagonalization matrix. The eigenvalues are related to the harmonic frequencies through

$$\omega_i^2(\mathbf{R}_0) = \lambda_i(\mathbf{R}_0), \quad (2)$$

and the unitary matrix is composed of $6N$ eigenvectors of the form

$$[c_{x,i,1}, c_{y,i,1}, c_{z,i,1}, c_{rx,i,1}, c_{ry,i,1}, c_{rz,i,1}, c_{x,i,2}, c_{y,i,2}, \dots, \\ c_{x,i,n}, c_{y,i,n}, c_{z,i,n}, c_{rx,i,n}, c_{ry,i,n}, c_{rz,i,n}]$$

whose coefficients describe the contribution of each translational and rotational degree of freedom of each molecule n to mode i . We have replaced the numerical index $\mu = \{1, 2, \dots, 6\}$ with $\{x, y, z, rx, ry, rz\}$ to indicate the nature of the translational or rotational molecular coordinate associated with each coefficient.

The density of states is essentially a histogram of frequencies obtained over a large number of configurations:

$$\rho(\omega) = \left\langle \sum_{i=1}^{6N} \delta(\omega - \omega_i) \right\rangle. \quad (3)$$

By definition, when integrating from $-\infty$ to ∞ , the integrated density of states must equal $6N$, which implies that it has dimensions of number of states per unit frequency.

One of the notable features of INM methods is that a weighted density of states, based on the nature of the normal modes as expressed in their eigenvectors, can be obtained.¹⁷ For instance, the total density of states weighted by the contributions of rotation about the molecular x axis is

$$\rho^{rx}(\omega) = \left\langle \sum_{i=1}^{6N} w_i^{rx} \delta(\omega - \omega_i) \right\rangle, \quad (4)$$

where the weighting factor w_i^{rx} is the square of the projection of the eigenvector onto the coordinates corresponding to rotation about the x axis of each molecule:

$$w_i^{rx} = \sum_{n=1}^N c_{rx,i,n}^2. \quad (5)$$

Given a distribution of eigenvalues, the most basic approximation to a FIR spectrum, which we will call method I, involves generating a weighted density of states according to the sum of the contributions to the mode by rotations about the x and y axis of each molecule. The dipole is oriented along the z axis, and rotations about this axis will not contribute to absorption,

$$w_i^I = \frac{1}{2} \sum_{n=1}^N \frac{\mu^2 c_{rx,i,n}^2}{I_{xx}} + \frac{\mu^2 c_{ry,i,n}^2}{I_{yy}}. \quad (6)$$

The μ^2/I_{xx} and μ^2/I_{yy} factors provide the average weight per mode. As discussed in Refs. 15 and 22, a factor of $(A')^2$ is used when weighting the density of states for a given quantity A , where A' is the derivative of the quantity of interest with respect to mode q , i.e., $(\partial A/\partial q)$. In the case of infrared active absorption, the quantity A' corresponds to the mass weighted dipole derivative. The factor of $1/2$ in Eq. (6) accounts for the fact that in an isotropic distribution the dipoles are not aligned, and the sum of μ^2 along any given direction for N randomly distributed dipoles will be $(1/2)N\mu^2$. The weighted density of states is then

$$\rho^I(\omega) = \left\langle \sum_{i=1}^{6N} w_i^I \delta(\omega - \omega_i) \right\rangle. \quad (7)$$

This approximation amounts to the assumption that the net dipole moment per unit volume is not dependent on the relative orientations of the molecules.

Method II is a more sophisticated treatment, in which modes are again weighted by the square of the change in permanent dipole moment they cause, but their vector sum is calculated before squaring,

$$w_i^{II} = \left(\frac{\partial |M_{\text{perml}}|}{\partial q_i} \right)^2 = \left| \sum_{n=1}^N \mu \left(\frac{c_{rx,i,n} \hat{e}_{xn}}{\sqrt{I_{xx}}} - \frac{c_{ry,i,n} \hat{e}_{yn}}{\sqrt{I_{yy}}} \right) \right|^2. \quad (8)$$

Here, q_i is the coordinate corresponding to motion along normal mode i , μ is the molecular dipole moment, \hat{e}_{xn} and \hat{e}_{yn} are the unit vectors along the x and y axes of molecule n , and I_{xx} and I_{yy} are the principal moments of inertia about the x and y axes, respectively. Unlike method I, method II takes into account the extent to which a mode with a given magnitude of rotational character is in fact IR-active, rather than assuming a mean value for the IR activity based solely on the amount of rotational character.

Methods I and II only take into account permanent dipoles, but it is also possible to incorporate the effects of electronic polarizability (e.g., dipole-induced dipole effects) into an INM weighting procedure, which we refer to as method III,

$$w_i^{\text{III}} = \left(\frac{\partial |\mathbf{M}_{\text{net}}|}{\partial q_i} \right)^2 = \left(\frac{\partial |\mathbf{M}_{\text{perm}} + \mathbf{M}_{\text{ind}}|}{\partial q_i} \right)^2. \quad (9)$$

The change in the permanent component of the net dipole derivative arises only from rotation about the molecular x and y axes, and is found in Eq. (8). The induced component, due to changes in electronic polarization, has contributions from both rotational and translational motions. The self-consistent calculation of the induced electronic polarization (within a point charge-point polarizability picture) requires an iterative procedure, but it can be approximated to first order as arising only from the permanent charge distribution. The first order dipole moment induced by interaction of two polarizable point charges at sites s and s' on identical molecules n and n' is

$$\mathbf{m}_{ns,n's'} = (\alpha_s \zeta_{s'} - \alpha_{s'} \zeta_s) \frac{(\mathbf{r}_{ns} - \mathbf{r}_{n's'})}{r_{ns,n's'}^3}, \quad (10)$$

where α is the site polarizability, ζ is the charge, and $r_{ns,n's'}$ is $|\mathbf{r}_{ns} - \mathbf{r}_{n's'}|$. The derivative of the induced dipole moment for this pair interaction with respect to an arbitrary coordinate q_i is then given by

$$\frac{\partial \mathbf{m}_{ns,n's'}}{\partial q_i} = \frac{(\alpha_s \zeta_{s'} - \alpha_{s'} \zeta_s)}{r_{ns,n's'}^3} \mathbf{T}_{ns,n's'} \left(\frac{\partial \mathbf{r}_{ns}}{\partial q_i} - \frac{\partial \mathbf{r}_{n's'}}{\partial q_i} \right), \quad (11)$$

where the tensor $\mathbf{T}_{ns,n's'}$ is defined by

$$\begin{aligned} \mathbf{T}_{ns,n's'} &= \mathbf{I} - 3\hat{\mathbf{r}}_{ns,n's'}\hat{\mathbf{r}}_{ns,n's'} \\ &= r_{ns,n's'}^{-2} \begin{bmatrix} r^2 - 3r_x^2 & -3r_x r_y & -3r_x r_z \\ -3r_x r_y & r^2 - 3r_y^2 & -3r_y r_z \\ -3r_x r_z & -3r_y r_z & r^2 - 3r_z^2 \end{bmatrix}_{ns,n's'}. \end{aligned} \quad (12)$$

Summing over all pairwise interactions gives a net change in induced dipole moment for mode i :

$$\frac{\partial \mathbf{M}_{\text{ind}}}{\partial q_i} = \sum_{n=1}^N \sum_{\substack{n'=1 \\ n' \neq n}}^N \sum_{s=1}^S \sum_{s'=1}^S \frac{(\alpha_s \zeta_{s'} - \alpha_{s'} \zeta_s)}{r_{ns,n's'}^3} \mathbf{T}_{ns,n's'} \frac{\partial \mathbf{r}_{ns}}{\partial q_i}. \quad (13)$$

The last term on the right-hand side of Eq. (13) includes mass-weighted contributions from the translational and rotational coefficients of mode i corresponding to molecule n :

$$\begin{aligned} \frac{\partial \mathbf{r}_{ns}}{\partial q_i} &= \begin{bmatrix} \frac{c_{i,n,x}}{\sqrt{m}} \\ \frac{c_{i,n,y}}{\sqrt{m}} \\ \frac{c_{i,n,z}}{\sqrt{m}} \end{bmatrix} + [\hat{\mathbf{e}}_{xn} \times \mathbf{v}_{n,s} \quad \hat{\mathbf{e}}_{yn} \times \mathbf{v}_{n,s} \quad \hat{\mathbf{e}}_{zn} \times \mathbf{v}_{n,s}] \\ &\quad \times \begin{bmatrix} \frac{c_{i,n,rx}}{\sqrt{I_{xx}}} \\ \frac{c_{i,n,ry}}{\sqrt{I_{yy}}} \\ \frac{c_{i,n,rz}}{\sqrt{I_{zz}}} \end{bmatrix}. \end{aligned} \quad (14)$$

Here, $\hat{\mathbf{e}}_{xn} \times \mathbf{v}_{n,s}$ is the cross product of the unit vector along the x axis of molecule n with the vector from the center of mass to site s on the same molecule n .

B. Calculation of FIR spectra

Keyes¹⁵ has related the density of INM modes weighted according to their influence on a dynamical variable to the time correlation function of that variable, as specified here for the case of the net dipole moment

$$\begin{aligned} \langle \mathbf{M}(t) \cdot \mathbf{M}(0) \rangle &= \langle \mathbf{M}_i \cdot \mathbf{M}_i \rangle \\ &\quad + k_B T \int_{-\infty}^{\infty} d\omega \langle \rho^M(\omega) \rangle \omega^{-2} \cos(\omega t), \end{aligned} \quad (15)$$

where $\mathbf{M}(t)$ is the net dipole at time t , \mathbf{M}_i is the dipole moment at the potential minimum of mode i , k_B is Boltzmann's constant, and T is temperature. The first term on the right-hand side is not relevant at non-zero frequencies, and can be ignored when calculating spectra. Note that the density of states $\langle \rho_{\alpha}^M(\omega) \rangle$, normally calculated with all frequencies assigned to be positive, must be reduced by a factor of 2 to account for the inclusion of negative (not to be confused with imaginary) frequencies in the integral.

The procedure commonly used for comparison of MD simulation results with FIR data¹¹ calls for the Fourier transform of the net dipole time correlation function

$$\begin{aligned} \alpha(\nu)n(\nu) &= \frac{16\pi^3 \nu}{3hc} \tanh(h\nu/2k_B T) \frac{1}{V} \\ &\quad \times \int_{-\infty}^{\infty} dt \exp(-2\pi i \nu t) \langle \mathbf{M}(t) \cdot \mathbf{M}(0) \rangle, \end{aligned} \quad (16)$$

where $\alpha(\nu)$ is the frequency-dependent absorption coefficient in Nepers/cm, $n(\nu)$ is the frequency-dependent index of refraction, $\nu = \omega/2\pi$, h is Planck's constant, c is the speed of light, k_B is Boltzmann's constant, T is temperature and V is the volume of the sample. Fourier transform and substitution of Eq. (15) into Eq. (16) yields

TABLE I. Tabulation of site–site potential parameters used in MD simulations. All parameters were obtained from literature models except for polarizability. For water and ammonia, the mean (isotropic) gas-phase polarizability was assigned to the central atom, while for chloroform the polarizability was assigned in a manner qualitatively consistent with the polarizabilities in the series CH_4 , CH_3Cl , CH_2Cl_2 , CHCl_3 , CCl_4 assuming additivity for polarizability of carbon and chlorine atoms.

Liquid	Charge		Lennard-Jones parameters		Bond lengths (Å)	Polarizability (Å ³) ^a
	(e)		C ₆ (kJ Å ⁶ mol ⁻¹)	C ₁₂ (kJ Å ¹² mol ⁻¹)		
$\text{H}_2\text{O}^{\text{b}}$	O 0	O–O	2512	2910×10^3	O–H 0.9572	O 1.47
	H 0.535			H–H 1.514		
	M –1.070				O–M ^c 0.150	
NH_3^{c}	N 0	N–N	7170	1107×10^3	N–H 1.0124	N 2.25
	H 0.462				H–H 1.6243	
	M –1.386				N–M ^c 0.156	
CHCl_3^{d}	C 0.179	C–C	2630.9	4064×10^3	C–Cl 1.758	C 2.3
	Cl –0.087	C–Cl	4675.4	7481×10^3	Cl–Cl 1.676	Cl 2.4
	H 0.082	C–H	362.2	174.5×10^3	C–H 1.100	
		Cl–Cl	8306.7	13765×10^3		
		Cl–H	649.3	326.6×10^3		
		H–H	37.7	4.3×10^3		

^aPolarizability used only for calculating net dipole moment, not for intermolecular forces.

^bReference 23.

^cReference 24.

^dReference 25.

^eSite M is on symmetry axis, displaced towards hydrogens.

$$\alpha(\nu)n(\nu) = \frac{4\pi k_B T}{3h\nu c} \tanh(h\nu/2k_B T) \frac{1}{V} \langle \rho^M(\nu) \rangle. \quad (17)$$

Strictly speaking, Eqs. (15) and (17) are only valid in the absence of modes with imaginary frequencies. We have found, however, that it is necessary to treat modes with imaginary frequencies analogous to those with real frequencies when computing $\langle \rho^M(\nu) \rangle$ for use in Eq. (17) to better reproduce the low frequency region of FIR spectra. This point will be further discussed in Section IV.

III. COMPUTATIONAL AND EXPERIMENTAL DETAILS

A. MD simulations and INM analysis

Molecular dynamics simulations were performed using rigid, site-site, non-polarizable molecular potentials taken from the literature for water,²³ ammonia,²⁴ and chloroform,²⁵ details are given in Table I. The method of Berendsen *et al.*²⁶ was used as a thermostat, with a time constant of 500 fs. The Verlet algorithm was used,²⁷ and a reaction field incorporated to account for long-range electrostatic interactions,²⁸ with the effective dielectric constant of the surroundings (ϵ_{RF}) set equal to the known experimental static dielectric constant for the liquid.

Contributions to the net dipole vector of the system from the permanent molecular dipole moment and from a first-order estimate of the dipole-induced electronic polarization (calculated using the site polarizabilities shown in Table I) were computed every ten time-steps and used to calculate a net dipole time-correlation function. The gas-phase values of the permanent dipole moment,²⁹ rather than the enhanced values such as incorporated into the water and chloroform

models for use in liquid simulations,^{23,25} were used to calculate the timecorrelation function and the INM treatment of the FIR spectrum for all liquids.

INM eigenvalues and eigenvectors were calculated for ten configurations of each liquid generated during the course of the MD simulations. Depending on the liquid, this allowed from 5 to 50 Debye time constants to elapse between configurations used for the INM calculations.

B. Experimental FIR spectra

Sub-picosecond FIR pulse spectroscopy was used to measure the frequency-dependent absorption coefficient $\alpha(\nu)$ and index of refraction $n(\nu)$ of water, chloroform, and liquid ammonia at room temperature. Experimental details are as given in Ref. 7, except that the fs THz receiver substrate was low-temperature MBE-deposited GaAs. The variable pathlength cell described in Ref. 7 was used to obtain data for water over a range of pathlengths from 0.1 to 0.7 mm, and for chloroform from 1.6 to 4.0 mm. The vapor pressure of liquid ammonia is roughly 10 atmospheres at room temperature, which precluded the use of our variable pathlength cell. Instead, room-temperature liquid ammonia was contained in equilibrium with its vapor in a stainless steel pressure cell with 3 mm thick quartz windows. Transmission measurements were obtained using Teflon spacers of different thickness (0.050 mm, 0.127 mm, and 0.229 mm) to vary the pathlength, and the data were used to derive optical constants in the region covering 4 cm^{-1} to 50 cm^{-1} .

TABLE II. Conditions used for the MD simulation.

Liquid	N	Density (g/ml)	T (K)	time step (fs)	total time (ps)	ϵ_{RF} (reaction field)
H ₂ O	125	1.00	303	1.29	257.6	78.0
NH ₃	125	0.60	294	1.29	257.6	16.0
CHCl ₃	125	1.47	297	2.58	515.2	4.8

IV. RESULTS AND DISCUSSION

A. Analysis of time-domain MD results

MD simulations on liquid water, ammonia, and chloroform were carried out under the conditions described in Table II. The net dipole time correlation function $\langle \mathbf{M}(t) \cdot \mathbf{M}(0) \rangle$ calculated from MD simulation of simple models of liquid water, ammonia, and chloroform is shown in Figure 1. This function, which describes the transverse dielectric response of the liquid,³⁰ was calculated with and without the inclusion of dipole-induced electronic polarization. The magnitude of the time correlation function at $t=0$ is the mean square dipole moment per unit volume, which is proportional to the static dielectric constant. Under reaction field conditions, in which the liquid is modeled as if surrounded by a continuous medium of dielectric constant ϵ_{RF} , the static dielectric constant ϵ is determined through the equation²⁸

$$(\epsilon - 1) \left(\frac{2\epsilon_{\text{RF}} + 1}{2\epsilon_{\text{RF}} + \epsilon} \right) = \frac{4\pi(\langle \mathbf{M} \cdot \mathbf{M} \rangle - \langle \mathbf{M} \rangle \cdot \langle \mathbf{M} \rangle)}{3Vk_B T}. \quad (18)$$

Using Eq. (18), values of $\epsilon=33.4$, 9.8, and 2.1 were calculated for the water, ammonia, and chloroform, respectively using only permanent dipole moments; these increased to 50.3, 12.5, and 2.4 when the first-order approximation to the electronic polarization was included. As shown in Table III, these values are quite low in comparison with experiment, but consistent with reported results for similar or identical interaction potentials.^{28,31}

Each time-correlation function shows an inertial component at the very shortest times followed by a roughly exponential decay. The time constant of this decay, τ , is related to the Debye relaxation time, τ_D as follows:²⁸

$$\tau_D = \left(\frac{2\epsilon_{\text{RF}} + \epsilon}{2\epsilon_{\text{RF}} + 1} \right) \tau. \quad (19)$$

The calculated Debye times of 5.3 ps (H₂O), 0.62 ps (NH₃), and 5.1 ps (CHCl₃) are all close to values experimentally derived from frequency-dependent complex dielectric constants of these liquids.^{7,32,33} These Debye times are not affected by the inclusion of polarizability in the analysis, indicating that relaxation of the electronic polarization (which can occur through translational as well as orientational motion) is occurring on the same time scale as reorientation of the permanent dipoles. Better statistics will be required to determine whether the liquid models show secondary dielectric relaxation processes, as observed experimentally^{7,33} and in simulations with a different potential²⁸ in the case of water.

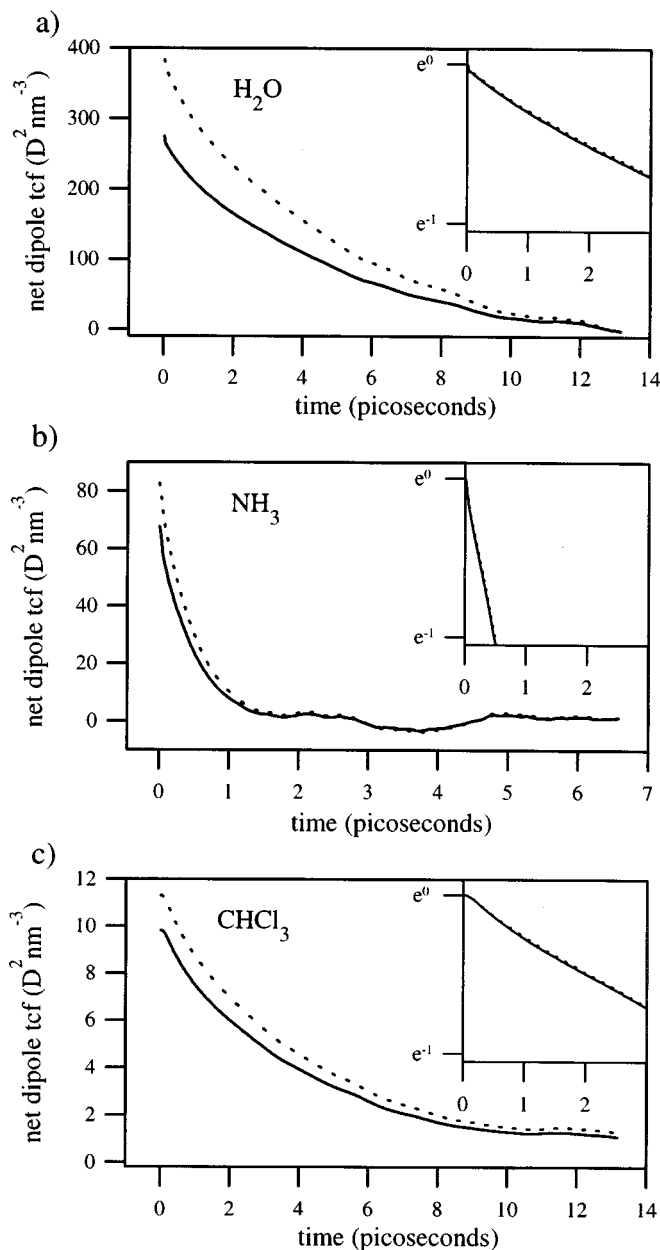


FIG. 1. The net dipole time correlation function, $\langle \mathbf{M}(t) \cdot \mathbf{M}(0) \rangle$ per unit volume, from MD simulations of (a) water, (b) ammonia, and (c) chloroform. Solid lines show relaxation of the permanent molecular dipoles only, and dotted lines show relaxation of the total dipole (the vector sum of permanent and induced dipoles). Insets show the exponential character of the decay on a normalized semi-log plot.

TABLE III. Results of the MD simulation.

Liquid	ϵ , permanent dipoles only	ϵ , polarizable model	ϵ , expt. ^a	τ_D , calc.	τ_D , expt.	Gas phase dipole moment ^d
H ₂ O	33.4	50.3	76.6 (303 K)	5.3 ps	8.2 ps ^b	1.85 D
NH ₃	9.84	12.5	16.9 (298 K)	0.62 ps	0.54 ps ^c	1.47 D
CHCl ₃	2.1	2.3	4.8 (293 K)	5.1 ps	5.4 ps ^d	1.01 D

^aReference 29.^bReferences 7, 33.^cJ. T. Kindt and C. A. Schmuttenmaer (unpublished).^dReference 32.

B. INM densities of states

The INM densities of translational and rotational states of liquid water, chloroform, and ammonia are shown in Figure 2. There are significant differences among these spectra which illustrate very basic properties of these liquids. The first is that the band extends to much higher frequencies, indicating faster librational dynamics, for water and ammonia than for chloroform. This is easily understood in terms of the lighter mass and much lower moments of inertia of the fully protonated solvents. A second noticeable difference is in the proportion of stable and unstable modes, i.e., modes with real and imaginary frequencies. Water shows the smallest proportion of unstable modes over all, and in its rotational components particularly, consistent with its highly organized hydrogen-bonded structure. In the case of water, our results match closely those of Cho *et al.*,¹⁸ except that they found an even smaller portion of unstable rotational modes; this discrepancy might be due to minor differences in simulation conditions.³⁴ Ammonia, with only one hydrogen bond acceptor and three donor sites, has a much looser framework and shows many more unstable rotational modes. The lower structural stability of ammonia with respect to water comes as no surprise, given that it is fifty degrees above its normal boiling point. Chloroform, which cannot form strong hydrogen bonds, has the weakest orientational structure and the highest proportion of unstable to stable modes. Chloroform is also distinct in that there is almost no frequency separation between its translational and rotational motion. Its large moments of inertia bring rotational frequencies into overlap with translational frequencies (which are roughly the same for all three liquids).

The distribution of Debye relaxation times in these liquids can be easily rationalized in terms of their INM spectra. The low structural stability of ammonia leads to a much shorter τ_D than that of water. In chloroform, on the other hand, the effects of low structural stability and slow overall dynamics cancel to give a relaxation time comparable to that of water.

C. Calculation of FIR absorbance spectra

Using Eqs. (16) and (17), we have calculated absolute FIR absorption spectra from the time correlation functions of Fig. 1, and from the weighted INM densities of states. Results are given as the product of the absorption coefficient $\alpha(\nu)$ and the frequency-dependent index of refraction

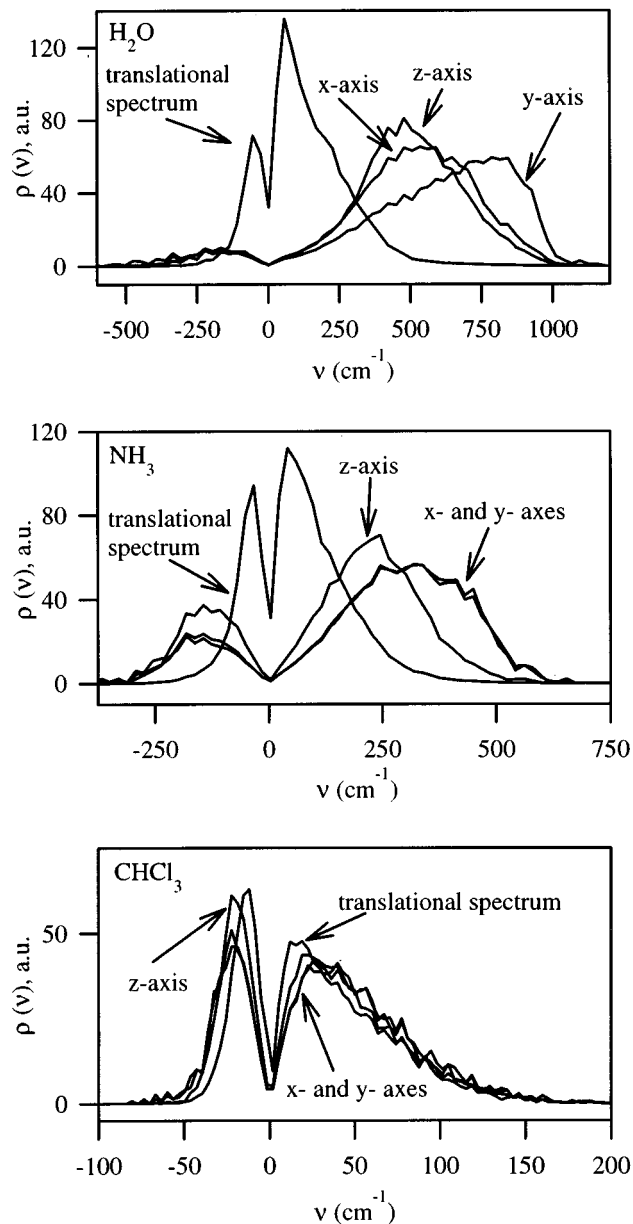


FIG. 2. INM densities of states projected onto the molecular translational and rotational coordinates, as in Eq. (4). The negative X-axis of the plot represents unstable modes with imaginary frequencies. The translational spectrum is an average over the 3 translational degrees of freedom, while the rotational spectrum is separated according to rotation about the x, y, and z molecular axes. For all liquids, the z axis is the dipolar axis. For H₂O, we define the y axis to be in the plane of the molecule.

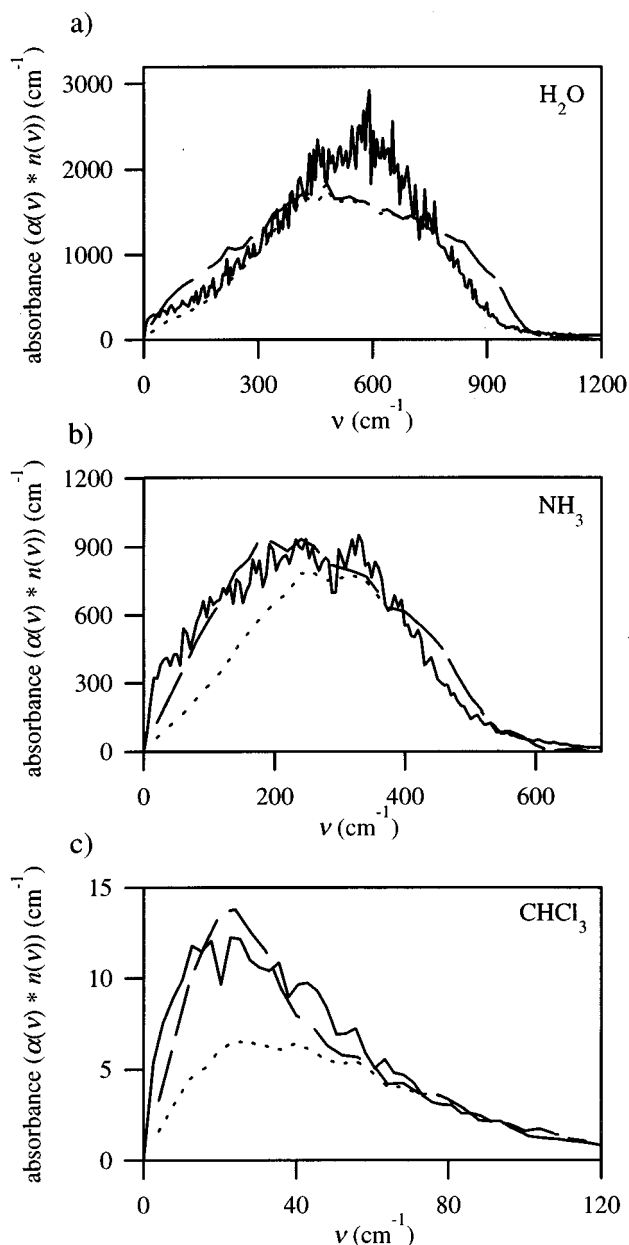


FIG. 3. Simulated FIR absorption spectra, including the effects of permanent dipoles only for (a) water, (b) ammonia, and (c) chloroform. The solid lines are calculated from the permanent dipole time correlation function of Fig. 1 by Eq. (16). The dotted and dashed lines are spectra generated from INM analysis using weighting method I and Eq. (17). The dotted lines include only modes with real frequencies, while the dashed lines include modes with imaginary frequencies treated as modes with real frequencies.

$n(\nu)$, following the form of Eq. (16). Figures 3 and 4 show spectra calculated using methods I and II, respectively. The solid lines indicate the spectra calculated from the time correlation functions, the dashed lines represent the weighted INM density of stable modes and unstable modes, with imaginary frequencies treated as real, and the dotted lines represent the weighted INM density of stable modes only. At low frequencies, there is a considerable deficit in absorbance calculated using only stable INM modes (dotted lines) relative to the exact absorbance (solid lines) calculated by the

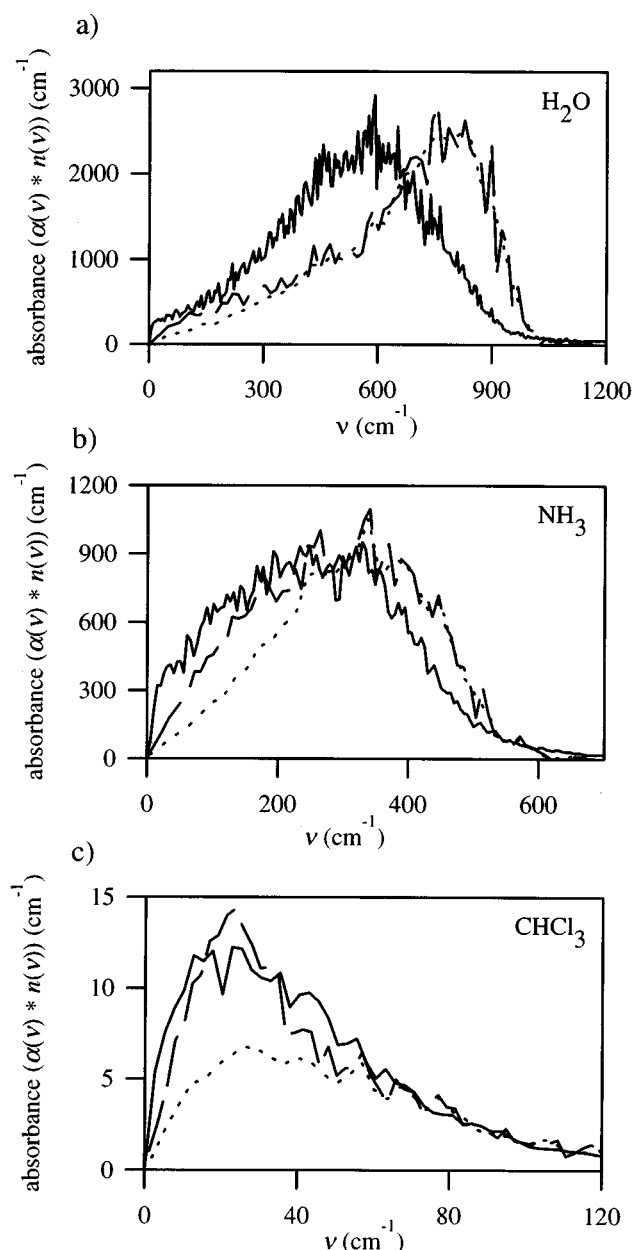


FIG. 4. Same as Figure 3, except using INM method II.

time-domain analysis of Eq. (16). Inclusion of only the real INM modes limits the spectrum to absorbance by oscillatory motion rather than relaxational motion. It is not surprising that the maximum of this deficit for each liquid corresponds roughly to the amount of absorbance at the Debye plateau³⁵

$$\lim_{\nu \rightarrow \infty} \alpha(\nu)n(\nu) = \frac{\epsilon - 1}{c\tau_D}, \quad (20)$$

since the Debye model describes relaxational motion only. Equation (20) yields 204 Np/cm for water, 475 Np/cm for ammonia, and 7 Np/cm for chloroform when calculated using the values of ϵ and τ_D derived from the results for the MD simulation with permanent dipoles only, shown in Table III. In order to correctly account for the absorbance associ-

ated with Debye relaxation, one approach would be to generate a time correlation function from the INM spectrum, multiply that function by an appropriate exponential decay factor, and then Fourier transform back again to the frequency domain. We felt that it would be more physically instructive, however, to consider how the unstable modes themselves might contribute to the absorbance. Including the unstable INM modes brings the spectra significantly closer in agreement for ammonia and chloroform. What may actually seem surprising is that this procedure works at all, given that Eq. (15) is based on the assumption of oscillatory dynamics, which will not hold for the unstable modes. That is, inclusion of imaginary frequencies in Eq. (15) results in an unphysical divergent time correlation function.

Treating imaginary frequencies and real frequencies equivalently for the purpose of calculating a FIR spectrum is tantamount to the assertion that some aspect of the dynamics relevant to absorption of energy from an oscillating electric field will be the same for motion in a harmonic potential well and motion on a barrier of equal and opposite curvature. Here we offer qualitative support for this assertion. The work per unit time, denoted W , done on a dipole by a time-dependent field is³⁶

$$W = -(1/\tau) \int_0^\tau dt E(t) \dot{m}(t), \quad (21)$$

where $E(t)$ is the time-dependent electric field, $m(t)$ is the time-dependent dipole moment of the sample, and $\dot{m}(t)$ is its first derivative with respect to time. If $E(t)$ and $m(t)$ are both oscillatory with angular frequencies ω_E and ω_m , this integral will only be non-zero when $\omega_E = \omega_m$ (and $\tau \gg 1/\omega_E, 1/\omega_m$). If $m(t)$ is not oscillatory and $\dot{m}(t)$ is not a sinusoidal function of time, as is the case on an unstable potential surface, the absorbance spectrum will depend on the time limits of integration of Eq. (21).

It is instructive to compare $m(t)$ and $\dot{m}(t)$ for the case of barrier crossing with the more familiar case of oscillatory motion in a parabolic well, as shown in Figure 5. We use position to refer to $m(t)$ and velocity for $\dot{m}(t)$. Both the position and velocity are sinusoidal for a stable mode, as shown in part a. There are two possibilities when considering the unstable modes. The first corresponds to a successful barrier crossing, shown in part b, that occurs when there is sufficient kinetic energy to cross the barrier. In this case, the velocity decreases as it goes up the barrier, and then increases on the way down. For an unsuccessful barrier crossing, the velocity decreases as it goes up the barrier, goes through zero when it comes to a stop and turns around, and then increases in the negative direction as it goes back down the barrier. For successful barrier crossing, the velocity is described by the hyperbolic cosine function, and the velocity for an unsuccessful crossing attempt is described by the hyperbolic sine function.

For a successful barrier crossing event, $\dot{m}(t)$ does not change sign, and the integral in Eq. (21) will be a maximum at DC frequencies. For an unsuccessful crossing, the spectrum will be peaked at a value of $\omega_E \approx (\pi/\tau)$ [or equiva-

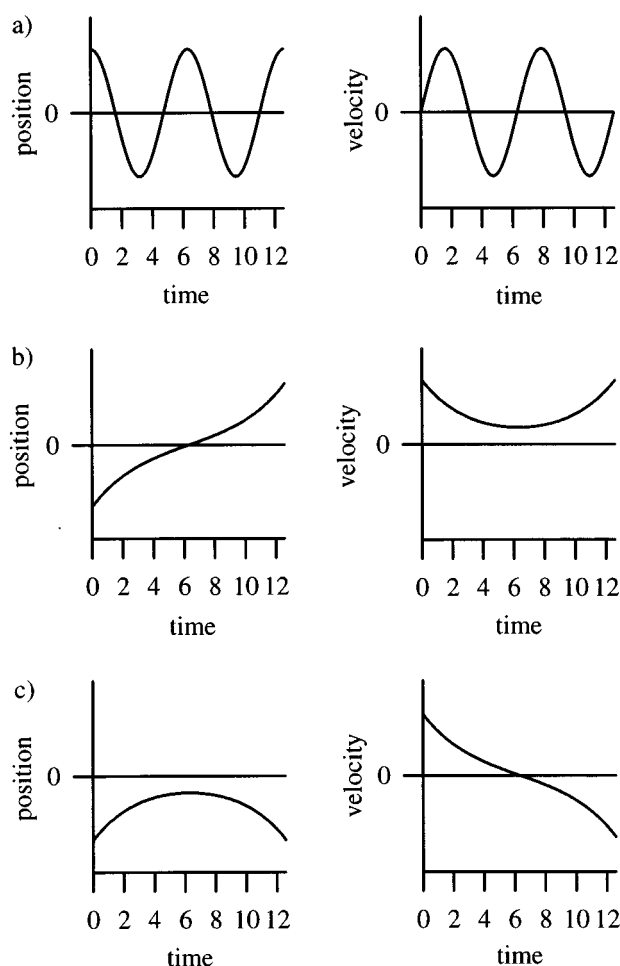


FIG. 5. Comparison of $m(t)$ and $\dot{m}(t)$ (referred to as position and velocity) for a stable mode and an unstable mode. Part (a) displays the harmonic motion in a parabolic well. Part (b) describes the case in which the barrier of an inverted parabola is crossed. Part (c) depicts the case of an unsuccessful barrier crossing attempt.

lently, $\nu_E \approx (1/2\tau)$ where τ is the time spent on the unstable surface. This can be understood qualitatively by considering part c of Figure 5. There will be maximum overlap between $E(t)$ and $\dot{m}(t)$ when the time along the abscissa is equal to half a period of $E(t)$, and when the phases are such that the E-field crosses through zero coincident with the velocity crossing through zero. For a given barrier height and energy of approach, the time spent on the barrier will also be inversely proportional to the magnitude of the imaginary frequency of the unstable mode (given by $|\omega_i| = \sqrt{-\partial^2 V / \partial q^2}$). From this we see there will be a direct proportionality between the magnitude of the imaginary frequency and the peak of the absorption spectrum associated with at least some of the unstable modes.

To approximate the constant of proportionality, we assume that any populated region of negative quadratic curvature in potential energy must be reasonably close to the potential maximum, because if it were far from the maximum, the force directed away from the center of the barrier would be too strong to allow population for any significant period

of time. The distribution of kinetic energy tells us that the displacement of stable modes from their potential minima is similarly limited. We know also that, when the system “rolls off” the barrier region, it will encounter a stable region before the kinetic energy of the mode becomes much greater than $k_B T$. It is evident that any motion in a dense, disordered equilibrium system will not be allowed to accelerate to far greater than the average velocity. Thus, we need to consider the frequency spectrum for absorbance due to barrier crossings and attempted barrier crossings within a range of roughly $q_i = 2(k_B T/\omega_i^2)^{1/2}$ of the barrier maximum. For a successful crossing the time spent on the barrier is

$$t = \frac{2}{\omega_i} \cosh^{-1} \left(\sqrt{\frac{KE_0}{KE_0 - E_b}} \right), \quad (22)$$

and for an unsuccessful attempt, it is

$$t = \frac{2}{\omega_i} \sinh^{-1} \left(\sqrt{\frac{KE_0}{E_b - KE_0}} \right), \quad (23)$$

where KE_0 is the initial kinetic energy, and E_b is the barrier height. For a successful crossing beginning with kinetic energy $2k_B T$, or an unsuccessful crossing beginning with kinetic energy $0.5k_B T$ encountering the same barrier with height $k_B T$, the time τ spent on the barrier is $1.76/\omega_i$. For an unsuccessful crossing, the absorption peak would be close to $\omega_E \approx (\pi/\tau) = \pi/(1.76/\omega_i) = 1.78\omega_i$. The time τ will increase and the frequency will decrease as the entering kinetic energy approaches the barrier height, from above or from below, giving a distribution in absorbance spectra which will at least include ω_i . As mentioned above, for successful barrier crossings the absorbance is greatest when the E-field is essentially constant during the motion, which will be true as $\omega_E \rightarrow 0$. For these reasons, a distribution extending from about $2\omega_i$ to lower frequencies, which is skewed toward lower frequencies, might be more appropriate than a delta function at ω_i to express the mean absorption spectrum of imaginary mode i . Such a distribution would probably help make up for the shortfall in absorbance at very low frequencies that persists when the unstable modes are treated as though they will cause maximum absorption at $\omega_E = \omega_i$. For the remainder of the paper, however, we shall incorporate the unstable modes as if they were stable modes when generating spectra.

At the high frequency side of the spectrum, the agreement of the INM result with the MD result varies with the different liquids. Furthermore, it is seen that method I performs slightly better than method II. For chloroform, the INM analysis, reproduces the shape and intensity of the band quite well, including the high-frequency tail. In ammonia, there is a moderate overestimate of absorption intensity above 400 cm^{-1} , while for water there is a severe discrepancy at frequencies above 300 cm^{-1} . This last finding was surprising, given that we expected the INM method to improve generally at high frequencies. We note that our results are consistent with previous work for both the FIR spectrum calculated from the MD simulation¹¹ and the INM rotational density of states.¹⁸ Comparison of the areas of disagreement

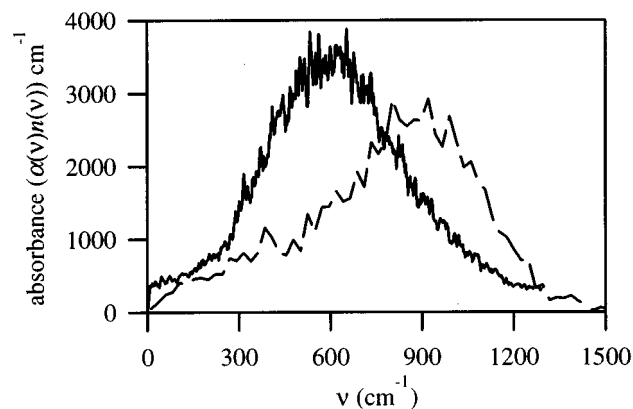


FIG. 6. Simulated FIR spectra of liquid hydrogen fluoride (HF) at 300 K. Solid line is from time-domain analysis, and dashed line is INM result using method II, as in Fig. 4.

with the distribution of rotational density of states suggests the discrepancy is related either to an overestimate of absorption related to rotation about the molecular y axis relative to the molecular x axis, or to an overestimate of the frequencies corresponding to rotation about the y axis. Here, in keeping with earlier INM studies of water¹⁸ we label the axis in the molecular plane the y axis; whereas using the standard convention for asymmetric top molecules, it would be the x axis because it has the smallest moment of inertia. The small moment of inertia of the y axis is largely responsible for the prominence of y -rotation at high frequencies in the INM spectrum. Since method I replicated the time-domain results more satisfactorily than methods II and III, we initially suspected that the more sophisticated INM treatment was not correctly accounting for the coupling between rotation about different axes in non-linear molecules. This hypothesis was disproved by additional MD simulations and INM analysis on liquid hydrogen fluoride, a molecule similar to water in many respects except in that it is linear. The potential of Cournoyer and Jorgensen was used.³⁷ Spectra of liquid HF determined from MD and INM analyses are shown in Figure 6. In HF as in H_2O , the FIR absorption band predicted by INM was shifted to significantly higher frequencies compared to the lineshape obtained from the time correlation function, indicating that rotational coupling about different axes is not an explanation for the discrepancy. Common features of water and hydrogen fluoride which might cause problems in the INM treatment are the small moments of inertia about one or more axes, and strong hydrogen bonding.

An assumption implicit to Eq. (15) which might also be related to the discrepancy is that the mean square amplitude of a given mode is related to its frequency by the relation¹⁵

$$[q_i^2] = k_B T / \omega_i^2, \quad (24)$$

which holds for systems of true harmonic oscillators. This assumption was investigated for the case of liquid water by Cho *et al.*¹⁸ who measured the mean square force along modes of a given frequency and observed a relationship in

which $[q_i^2] \propto 1/\omega_i^r$ with $r=2.88$ for stable modes, and $r=3.9$ for unstable modes. This is qualitatively consistent with the observed discrepancy. A decrease in mean square amplitude with respect to frequency that is more rapid than quadratic would lead Eq. (17), which assumes a quadratic weighting for ω in Eq. (24), to over-predict absorption at high frequencies with respect to low frequencies. However, the rescaling of the calculated results by $1/\omega^{0.88}$, or any other power of the frequency, does not give appreciably better overall agreement. Likewise, initial attempts to calculate $[q^2]$ as a numerical function of ω in order to correct Eq. (17) at each frequency, rather than assuming a simple power relation, were unable to improve the agreement between the time-domain and INM results.

D. Effects of electronic polarizability

Figure 7 shows the change in the calculated FIR spectrum when induced dipoles as well as permanent dipoles are included in the time-domain and INM analyses. Because the model for calculating electronic polarization utilizes the charge and polarizability of individual sites, there will be dipole-induced dipoles, quadrupole-induced dipoles, and higher order induced dipoles. The solid line in Fig. 7 is the difference between the spectra calculated with Eq. (15) using the two time correlation functions shown in Fig. 1, one of which is permanent dipoles only and the other of which includes induced dipole moments. The dashed line in Fig. 7 is the difference between the INM density of states weighted according to method III [Eqs. (9)–(14)] and method II [Eq. (8)]. The INM method successfully reproduces the trends and magnitudes of the time-domain calculations; the greatest discrepancies are clearly related to differences in the overall spectrum that were identified earlier, and not to the inclusion of induced dipoles. The water spectrum shows the most pronounced effects, with an increase in absorbance at low frequencies due in part to the activity of translational modes, and a strong cancellation effect of permanent and induced moments at higher frequencies leading to a decrease in absorption of over 40%. These effects were observed and discussed at length by Guillot.¹¹ The same trends, although not as pronounced, are observed in ammonia. The smaller effect on absorption when including polarizability in ammonia, which has a smaller dipole moment but a higher polarizability than does water, is probably related to both the lower density of liquid ammonia (0.6 g/cm^3 at 294 K) as well as the relative lack of structure, with a more isotropic environment and lower local electric fields. The same arguments account for the even smaller relative effect of induced dipoles on the FIR spectrum of chloroform, which does not show a cancellation effect.

E. Comparison of simulation results with experiment

Experimental values of $\alpha(\nu)n(\nu)$, measured using sub-ps FIR pulse spectroscopy, are shown in Figure 8 for comparison with MD time-domain and INM calculated spectra, including induced-dipole effects. Agreement in the case of water is good in the frequency range ($0\text{--}80 \text{ cm}^{-1}$) cur-

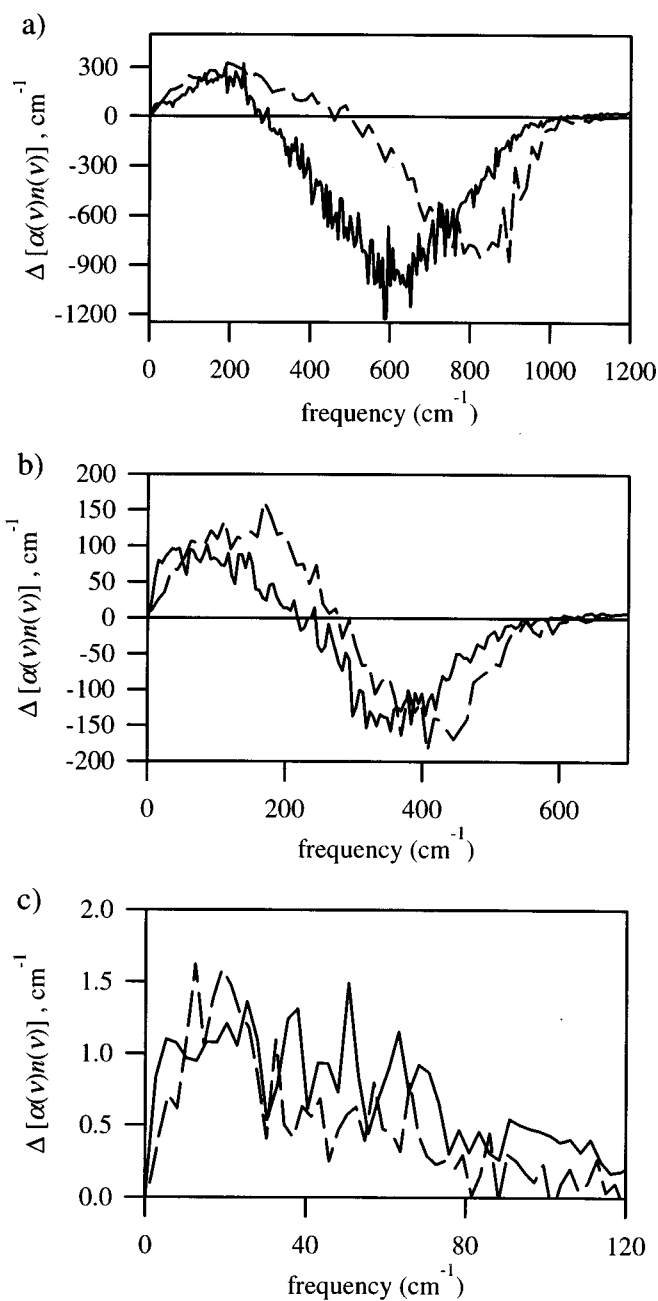


FIG. 7. Effect of induced dipole moments on calculated FIR spectra of (a) water, (b) ammonia, and (c) chloroform. Solid lines are time-domain results, representing the difference between the absorptivity calculated by Eq. (16) with and without the inclusion of induced dipoles. Dashed lines represent the difference between using INM method III and method II in calculating a weighted density of states for inclusion in Eq. (17). Positive values indicate increased absorbance when induced dipole moments are included.

rently accessible by the sub-ps FIR pulse technique. Data obtained at higher frequencies by conventional Fourier transform FIR spectroscopy have been published for water, and was reasonably well reproduced in MD simulations by Guillot only after a quantum correction procedure,¹¹ which we have not implemented. Agreement is poor in the accessible frequency range for liquid ammonia. This is probably related to the poor agreement between the calculated and experi-

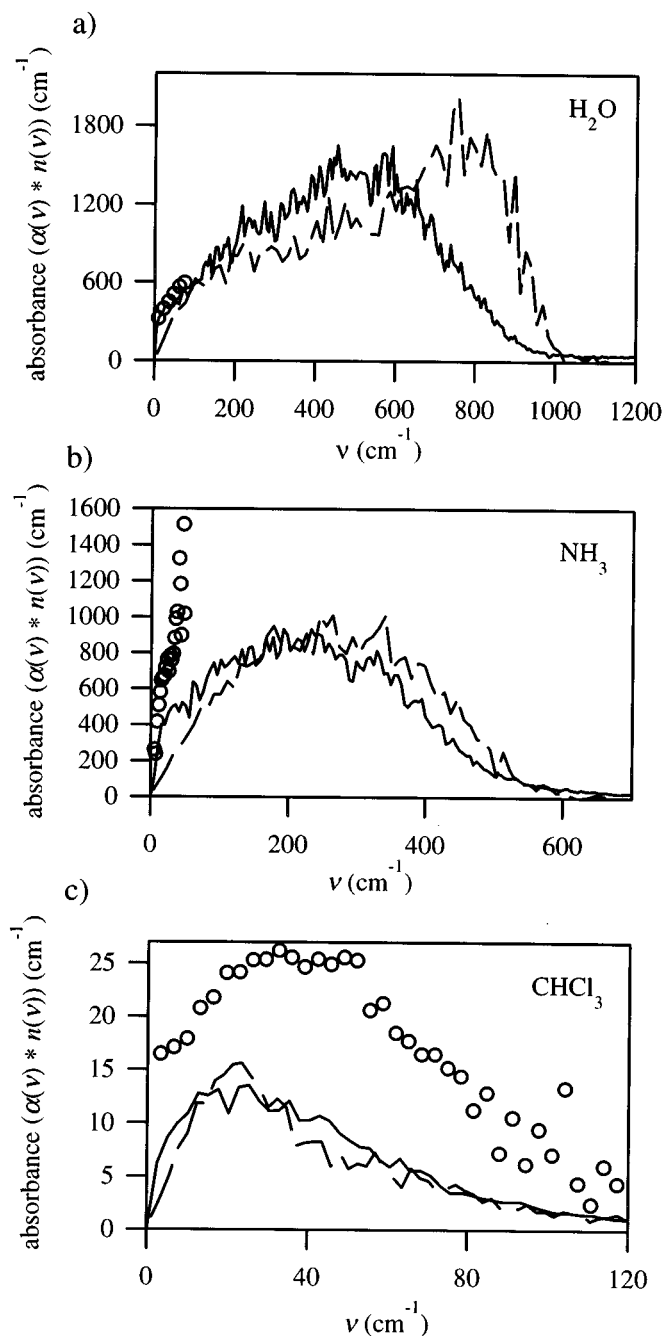


FIG. 8. Comparison of simulated and experimental FIR absorption spectra of (a) water, (b) ammonia, and (c) chloroform. Solid and dashed lines are calculated spectra, including permanent and induced dipole moments, generated from the MD and INM analyses, respectively. Open circles represent the product of the experimentally measured frequency-dependent absorption coefficient and index of refraction.

mental dielectric constant, which will result in a relatively large underestimate of the absorption associated with Debye relaxation. The fully polarizable ammonia model developed by Deng, Martyna and Klein,³⁸ which gives the correct static dielectric constant, might yield improved results. As for chloroform, which should not require significant quantum corrections over the major portion of its band ($h\nu \cong 0.2k_B T$

at its absorption maximum), the results are somewhat better, although overall absorbance is consistently underestimated by the model. We note that Flanders *et al.*⁸ fit the experimental FIR absorption spectrum of chloroform quite well up to 66 cm^{-1} with a sum of two Mori lineshapes, but this empirical analysis likewise underestimated the absorption at higher frequency. The inability of the molecular dynamics simulation to quantitatively duplicate the observed high-frequency absorbance suggests that the intermolecular potential must be further refined.

A particularly promising direction entails coupling the INM method with low frequency FIR dielectric measurements to investigate the effects of isotopic substitution on the rotational, translational, and hydrogen bonding dynamics in liquids such as water and ammonia. For example, hydrogen bonding dynamics in water could be more fully understood by measuring and calculating dielectric spectra below 50 cm^{-1} at a variety of temperatures in H_2O , D_2O , and their mixtures. A primary advantage of using the INM method is that it is easy to project out the contribution from modes participating in hydrogen bonding, and will allow trends to be uncovered.

V. CONCLUSIONS

We have used conventional MD time-domain methods and INM methods to simulate FIR spectra for liquid water, ammonia, and chloroform. The INM method, in addition to yielding general insight into the dynamics of these liquids, proved capable of nearly reproducing the absolute absorption spectrum obtained via the net dipole time correlation function from the MD simulation. When only stable modes were included in the analysis, a shortfall in low-frequency absorptivity was observed, and attributed to absorbance associated with Debye relaxation that can not contribute to a spectrum when only stable modes are used. We found empirically that including unstable modes on an equal footing with stable modes made up much of this difference and improved the overall fit significantly. Including induced dipole moments in the INM treatment led to the same trends as observed when including induced dipoles in the MD treatment. Overall agreement of experimental and simulated spectra using either method was relatively poor, suffering from the simplicity of the site-site potential models, the inexact treatment of induced dipole effects, and the lack of quantum corrections.

While the INM analysis did not yield the exact FIR spectrum for these liquid models, its ability to capture the basic features and trends makes it a useful interpretive tool, complementing or in some cases superseding the analysis of various correlation functions. The ability to physically describe or visualize a mode contributing to absorbance at a given frequency might be used, for instance: to yield insight into cancellation effects between permanent and induced dipole moments, to describe the effect of coupling among components in a solution or mixture, or to separate out the translational and rotational contributions to the induced-dipole spectrum. Finally, the capacity to use an instantaneous measurement to get at a FIR spectrum is indispensable if one

is to simulate experiments in which transient FIR spectra are observed following an excitation event, experiments conceivable with the use of sub-ps FIR pulses as an ultrafast probe.

ACKNOWLEDGMENTS

The authors would like to thank Profesor R. M. Stratt for helpful discussions. This work was partially supported by the Camille and Henry Dreyfus Foundation New Faculty Award Program and by a National Science Foundation Graduate Research Fellowship. Acknowledgment is made to the donors of The Petroleum Research Fund, administered by the ACS, for partial support of this research.

- ¹O. Faurskov Nielsen, *Annu. Rep. Prog. Chem. Sec. C* **90**, 3 (1993).
- ²D. McMorro, W. T. Lotshaw, and G. A. Kenney-Wallace, *IEEE J. Quantum Electron.* **24**, 443 (1988).
- ³Y. J. Chang and E. W. Castner, Jr., *J. Chem. Phys.* **99**, 113 (1993).
- ⁴H. P. Deuel, P. Cong, and J. D. Simon, *J. Phys. Chem.* **98**, 12 600 (1994).
- ⁵J. E. Pedersen and S. R. Keiding, *IEEE J. Quantum Electron.* **28**, 2518 (1992).
- ⁶L. Thrane, R. H. Jacobsen, P. Uhd Jepsen, and S. R. Keiding, *Chem. Phys. Lett.* **240**, 330 (1995).
- ⁷J. T. Kindt and C. A. Schmuttenmaer, *J. Phys. Chem.* **100**, 10 373 (1996).
- ⁸B. N. Flanders, R. A. Cheville, D. Grischkowsky, and N. F. Scherer, *J. Phys. Chem.* **100**, 11 824 (1996).
- ⁹B. Ladanyi, in *Spectroscopy and Relaxation of Molecular Liquids*, edited by D. Steele and J. Yarwood (Elsevier, Amsterdam, 1991), Chap. 10.
- ¹⁰D. M. F. Edwards, P. A. Madden, and I. R. McDonald, *Mol. Phys.* **51**, 1141 (1984); D. M. F. Edwards and P. A. Madden, *ibid.* **51**, 1163 (1984).
- ¹¹B. Guillot, *J. Chem. Phys.* **95**, 1543 (1991).
- ¹²H. Stassen and T. Dorfmueller, *Chem. Phys.* **187**, 337 (1994).
- ¹³I.M. Svishchev and P. G. Kusalik, *J. Chem. Soc. Faraday Trans.* **90**, 1405 (1994).
- ¹⁴R. M. Stratt, *Acc. Chem. Res.* **28**, 201 (1995).
- ¹⁵T. Keyes, *J. Chem. Phys.* **104**, 9349 (1996).
- ¹⁶B. M. Ladanyi and S. Klein, *J. Chem. Phys.* **105**, 1552 (1996).
- ¹⁷M. Buchner, B. M. Ladanyi, and R. M. Stratt, *J. Chem. Phys.* **97**, 8522 (1992).
- ¹⁸M. Cho, G. R. Fleming, S. Saito, I. Ohmine, and R. M. Stratt, *J. Chem. Phys.* **100**, 6672 (1994).
- ¹⁹T. Keyes, *J. Chem. Phys.* **101**, 5081 (1994).
- ²⁰G. V. Vijayadmodar and A. Nitzan, *J. Chem. Phys.* **103**, 2169 (1995).
- ²¹W. H. Press, S. A. Teukolsky, W. T. Vetterling, and B. P. Flannery, *Numerical Recipes in FORTRAN* (Cambridge, New York, 1992).
- ²²R. M. Stratt and M. Cho, *J. Chem. Phys.* **100**, 6700 (1994).
- ²³W. L. Jorgensen, *J. Chem. Phys.* **77**, 4156 (1982). This reference describes the TIPS2 potential.
- ²⁴R. W. Impey and M. L. Klein, *Chem. Phys. Lett.* **104**, 579 (1984).
- ²⁵W. Dietz and K. Heinzinger, *Ber. Bunsenges. Phys. Chem.* **88**, 543 (1984).
- ²⁶H. J. C. Berendsen, J. P. M. Postma, W. F. van Gunsteren, A. DiNola, and J. R. Haak, *J. Chem. Phys.* **81**, 3684 (1984).
- ²⁷M. P. Allen and D. J. Tildesley, *Computer Simulation of Liquids* (Clarendon, Oxford, 1987).
- ²⁸M. Neumann, *J. Chem. Phys.* **82**, 5663 (1985).
- ²⁹*CRC Handbook of Chemistry and Physics*, 71st ed., edited by D. R. Lide (Chemical Rubber, Boca Raton, 1990).
- ³⁰J. R. Birch and J. Yarwood, in *Spectroscopy and Relaxation of Molecular Liquids*, edited by D. Steele and J. Yarwood (Elsevier, Amsterdam, 1991), Chap. 5.
- ³¹I. G. Tironi and W. F. Van Gunsteren, *Mol. Phys.* **83**, 381 (1994).
- ³²A. A. Antony and C. P. Smyth, *J. Am. Chem. Soc.* **86**, 152 (1964).
- ³³J. Barthel, K. Bachhuber, R. Buchner, and H. Hetzenauer, *Chem. Phys. Lett.* **165**, 369 (1990).
- ³⁴The water simulation in this work used the same TIPS2 potential as was used in Ref. 18, but with half as many molecules, at 303 K rather than 298 K, and with reaction field rather than periodic lattice (Ewald sum) conditions. Furthermore, a 6 Å diam uncharged spherical solute was included in the other work.
- ³⁵J. R. Birch and J. Yarwood, in *Spectroscopy and Relaxation of Molecular Liquids*, edited by D. Steele and J. Yarwood (Elsevier, Amsterdam, 1991), pp. 174–273.
- ³⁶D. Chandler, *Introduction to Modern Statistical Mechanics* (Oxford, New York, 1987).
- ³⁷M. E. Cournoyer and W. L. Jorgensen, *Mol. Phys.* **51**, 119 (1984).
- ³⁸Z. Deng, G. J. Martyna, and M. L. Klein, *J. Chem. Phys.* **100**, 7590 (1994).